ELSEVIER

Polymer 43 (2002) 307–318

polymer

www.elsevier.com/locate/polymer

On permanent cilia and segregation in the crystallization of binary blends of monodisperse *n*-alkanes

I.L. Hosier, D.C. Bassett*

Department of Physics, J.J. Thompson Physical Laboratory, University of Reading, Whiteknights, P.O. Box 220, Reading RG6 6AF, UK

Received 15 June 2001; accepted 21 August 2001

Abstract

The isothermal crystallization kinetics and morphology have been investigated for a series of dilute binary blends using six monodisperse *n*-alkanes as guest in $C_{162}H_{326}$ as host. Two patterns of behaviour were observed. Guest molecules shorter than the host segregate as a separate population causing growth rates to become both reduced and non-linear. Morphologies are then noticeably less spherulitic than the host with less divergence between adjacent dominant lamellae but exhibiting no additional splaying at zero supercooling. By contrast, those blends with an *n*-alkane longer than the host co-crystallize (producing permanent cilia of controlled length) with a constant, but reduced, isothermal lamellar growth rate. Textures are now more spherulitic than the host, with additional splaying of an amount directly proportional to the number of permanent cilia and increasing with their length. The intercepts and slopes of plots of splaying data against supercooling are consistently related to permanent cilia plus inclined packing of initially rough lamellar surfaces and transient ciliation, respectively. The underlying causes of spherulitic growth for long molecules are thereby further confirmed and clarified.

Keywords: *n*-Alkane blends; Permanent cilia; Segregation

1. Introduction

Central and long-standing problems of spherulitic crystallization in polymers, the characteristic mode of self-organization and major determinant of properties have been much clarified in recent years by study of the monodisperse *n*-alkanes [1,2]. First, spherulitic growth has been shown to be associated with chainfolded, but not extended-chain growth of the same alkane [3,4]. This was anticipated from the earlier proposal [5–7] linking spherulitic growth to transient ciliation: only for the former will there be transient ciliation if molecular stems are assumed to add to the lamellae as a whole. Initially, transient ciliation was viewed as the uncrystallized portions of chains partly attached to a growing crystal, which by occupying space adjacent to a growing lamella, will tend to repel adjacent lamellae near the branch point causing them to diverge with linear traces. This concept was then widened [8] to include the excess of molecular length over that of the secondary nucleus to account for the onset of divergence of adjacent dominant lamellae at higher supercoolings in extended-chain crystallization. The measured angles of splay increase linearly with supercooling, but show a finite intercept at zero supercooling [9] when the nuclear and molecular lengths are equal, a finding which points to a second cause of splaying, suggested to be the inclined packing of initially rough basal surfaces and supported by the consistent scheme of interpretation of splaying plots spelled out in the present paper. Permanent, as opposed to transient, cilia may be introduced into a binary blend by co-crystallization of a longer guest molecule in a shorter host. This produces additional splaying (at zero supercooling) [10] but, on the other hand, when the longer guest was twice the length of the host so that its chainfolded length equalled that of the extended host, so excluding permanent cilia, the additional splaying was lost [11]. In combination, all this evidence has provided detailed confirmation of the central role of ciliation in producing spherulitic growth and also afforded an insight into how ciliation actually operates.

This paper now examines the consequences of varying the length of the guest molecule in $C_{162}H_{326}$ as host. Both shorter and longer guest molecules have been used. The former produce cellulation above their melting points and disrupt spherulitic growth in line with previous experience. The latter co-crystallize to give permanent cilia of controlled length. They show additional splaying (increased

* Corresponding author. Tel.: +44-118-931-8540; fax: +44-118-975-0203.

E-mail address: d.c.bassett@reading.ac.uk (D.C. Bassett).

0032-3861/02/$ - see front matter
PII: S0032-3861(01)00622-X

intercepts) at zero supercooling proportional to the number of permanent cilia and increasing with cilium length. Spherulitic textures are always enhanced by permanent cilia. Different aspects of the splaying data are shown to inform consistently on permanent cilia, transient ciliation and inclined packing of initially rough surfaces as factors contributing to the spherulitic growth of long molecules.

2. Experimental

Blends of monodisperse *n*-alkanes, synthesized by Dr G.M. Brooke and colleagues at the University of Durham after Whiting [1,2], have been prepared in binary sets with a total of six guest molecules, viz. $C_{48}H_{98}$ (C48), $C_{98}H_{198}$ (C98), $C_{122}H_{246}$ (C122), $C_{194}H_{390}$ (C194), $C_{210}H_{424}$ (C210) and $C_{246}H_{494}$ (C246) with $C_{162}H_{326}$ (C162) as common host. Such blends (B) are designated B48/10 to indicate, for example, that C48 is the guest with a concentration of 10 mol% and so on; exact proportions are listed in Table 1.

Some 20 mg of each blend was prepared by weighing the required amounts of each component on a Stanton DSC microbalance, dissolving each in 10 ml of 'Aristar' brand xylene and heating to the boiling point with continual stirring. The hot blend solution was then poured directly into about 10 ml of Aristar brand methanol (which had been pre-cooled over dry ice for about 10 min) inducing immediate precipitation of the blend which was filtered from the mixed solvent and dried under vacuum to constant mass.

2.1. Thermal analysis

A Perkin–Elmer DSC 2C, calibrated for scanning and isothermal runs using tin, indium, lead and stearic acid, was used for all DSC measurements. Crystallization was monitored as a function of time with samples of 1–2 mg, melted in the DSC at 134°C for 1 min then cooled at a rate of 40 K min^{-1} to the required crystallization temperature. Subsequent melting endotherms were recorded from room temperature to 140°C at a rate of 20 K min^{-1}. All data were corrected for the instrumental baseline and normalized to unit mass. To avoid degradation, a maximum of two crystallization/melting runs was performed on each sample and always under a nitrogen atmosphere.

Table 1
Blend compositions (experimental uncertainty in all determinations is ±0.1)

Blend	Guest alkane	Mol% guest	Mass% guest
B48/5	$C_{48}H_{98}$	5.1	1.7
B48/10	$C_{48}H_{98}$	10.4	3.3
B98/5	$C_{98}H_{198}$	5.2	3.2
B98/10	$C_{98}H_{198}$	9.6	6.1
B122/2	$C_{122}H_{246}$	2.6	2.0
B122/5	$C_{122}H_{246}$	6.7	5.5
B122/10	$C_{122}H_{246}$	12.7	9.8
B194/5	$C_{194}H_{390}$	5.0	5.9
B194/10	$C_{194}H_{390}$	9.9	13.2
B210/5	$C_{210}H_{424}$	4.9	6.3
B210/10	$C_{210}H_{424}$	9.9	12.4
B246/2	$C_{246}H_{494}$	1.8	2.6
B246/5	$C_{246}H_{494}$	3.4	5.4
B246/10	$C_{246}H_{494}$	8.3	12.0

2.2. Kinetics and optical microscopy

Five milligram samples, pressed between clean microscope slide and cover slip, were used for all optical and associated kinetic investigations. Crystal growth was observed directly between crossed polars using a Mettler FP-80 hot stage mounted on a Vickers Universal microscope. Ongoing crystallization was videotaped using a CCD camera attached to the microscope, which allowed the radius, or half-length, of individual crystals to be recorded as a function of time. The gradients of such plots gave the corresponding growth rates. The same crystallization protocol was followed as for the DSC procedure, viz. melting for 1 min at 134°C, then cooling at 40 K min^{-1} to the crystallization temperature; samples were quenched on a cold surface at the end of crystallization. Subsequent optical examination and photography were performed in transmission between crossed polars on a Zeiss Universal microscope; magnifications were calibrated against a standard graticule.

2.3. Transmission electron microscopy

About 1–2 mg of the required blend, placed on a standard 3.05 mm grid on a microscope slide, was melted on a Kofler WME hot bench for 1 min to remove any included air after which a cover slip was placed on top. Crystallization was effected by placing this whole assembly in a Mettler FP-80 hot stage at the required isothermal temperature. Following crystallization, the cover slip was removed and the sample etched for 10 min in a permanganic reagent composed of 1% w/v $KMnO_4$ in an acid mixture of 1 part water, 4 parts ortho-phosphoric acid and 10 parts sulphuric acid; the etchant was changed halfway through the procedure. The reaction was quenched by plunging samples in a mixture of 1 part H_2O_2 to 4 parts of an acid mix with 2 parts sulphuric acid to 7 parts water, which had been pre-cooled by standing over dry ice. The grid was then washed with methanol, gently removed from the slide and the etched sample allowed to dry. For direct replication, tungsten/tantalum metal was evaporated at ~35°, followed by vertical carbon coating. Residual specimen was removed by refluxing in boiling xylene after which the resulting replicas were ready for TEM examination.

2.4. Splaying angles

Crystal splaying angles were measured as previously [9–11], using suitably oriented (edge-on) adjacent, but distinct, lamellae chosen from TEM micrographs of each blend. A total of 30–40 such measurements per point gave a sensible

mean, which is little biased by any residual tilt of the crystals with respect to the ideal edge-on conditions required.

3. Results

3.1. Growth kinetics

3.1.1. Time dependence

The crystallization rates derived from DSC data agree with those obtained by direct measurement of the growth kinetics; accordingly, only the latter are presented here. They refer to isothermal crystallizations at temperatures appropriate for the host alkane C162, according to previous data [9].

The general features are that for all blends with a shorter guest *n*-alkane, the lamellar growth rate decreases with time, as shown in the example of Fig. 1a. This accompanies segregation of the shorter species, a result that is confirmed below by the DSC data. Conversely, all blends with a longer guest *n*-alkane show a constant isothermal growth rate until objects impinge (Fig. 1b) as does the host alkane C162 (Fig. 1c); this is associated with co-crystallization of both species. In the following data of average growth rate, only the initial gradient is taken for those blends that show time-dependent growth rates.

3.1.2. Shorter guest alkanes

Fig. 2a–c shows the initial growth rates, plotted as functions of crystallization temperature, for the pure host and its blends with the shorter alkanes C48, C98 and C122. The variation of growth rate with crystallization temperature in the available range is always very similar to that of the host *n*-alkane in all the blends: the characteristic dip, at the onset of branching [8,9], has been discussed in detail elsewhere [12] and is also reproduced in the blends. In all figures, there is a decrease in isothermal growth rate with increasing amounts of the same guest *n*-alkane, towards a lower value which may represent a diffusion limit: a minimum growth rate is observed for blends containing at least ~6% by mass of the guest alkane regardless of its molecular length. A comparison of different figures shows that curves are broadly similar for blend pairs B48/5 and B122/2, B48/10 and B98/5 and again for B98/10, B122/5 and B122/10.

Each of the above groups of blends has essentially the same mass percentage (mass%) but not the same molar percentage (mol%) of the guest alkane, i.e. approximately 1.5, 3, and between 5 and 10%, respectively (see Table 1). These data suggest that the reduction in growth rates depends only on the mass percentage of the guest alkane used, across the range of molecular lengths, to a point ($\geq$~6 mass%) where no further reduction in growth rate is observed.

3.1.3. Longer guest alkanes

Fig 2d–f shows the radial growth rates of the pure host and blends containing the longer guest alkanes C194, C210 and C246. The behaviour of these blends is more complex than hitherto in that it depends on both the total mass and length of the guest molecule. In view of the curves' complexity, consider first the part of the curve that is more or less flat, i.e. for temperatures below ~120°C. For

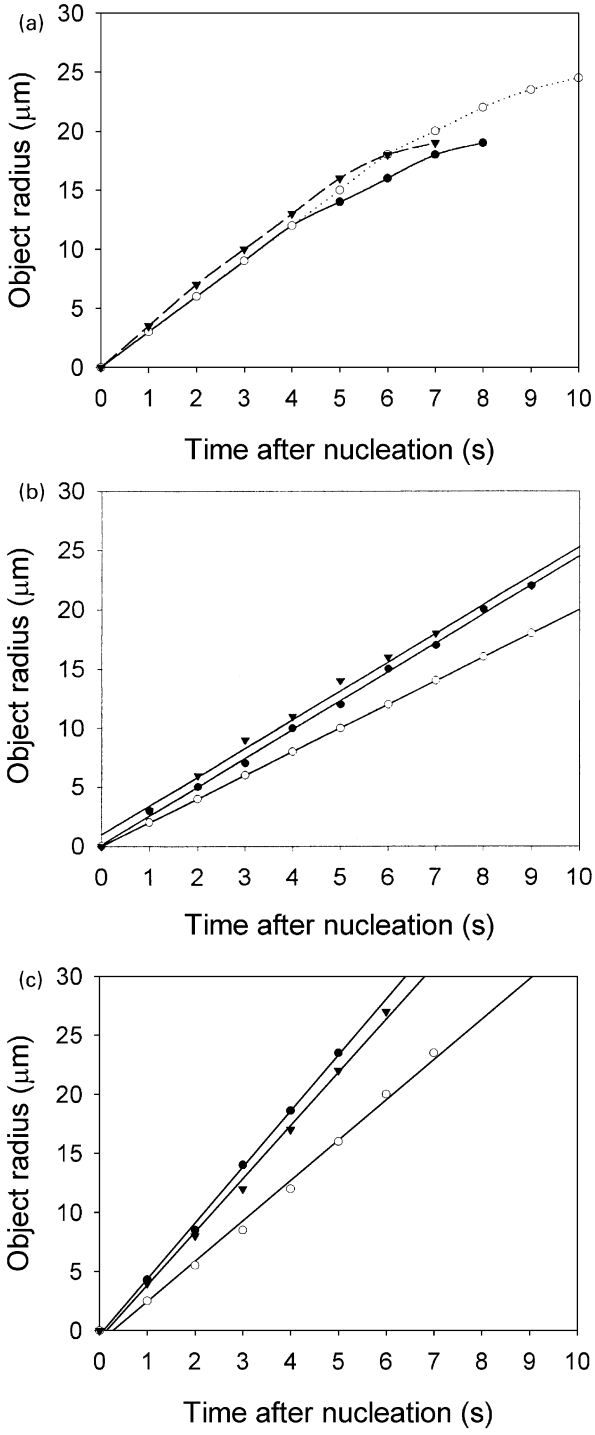

Fig. 1. Growth rate data for individual objects in blends crystallized at 120°C: (a) non-linear behaviour in B98/10; linear behaviour in (b) B210/10, and (c) C162.

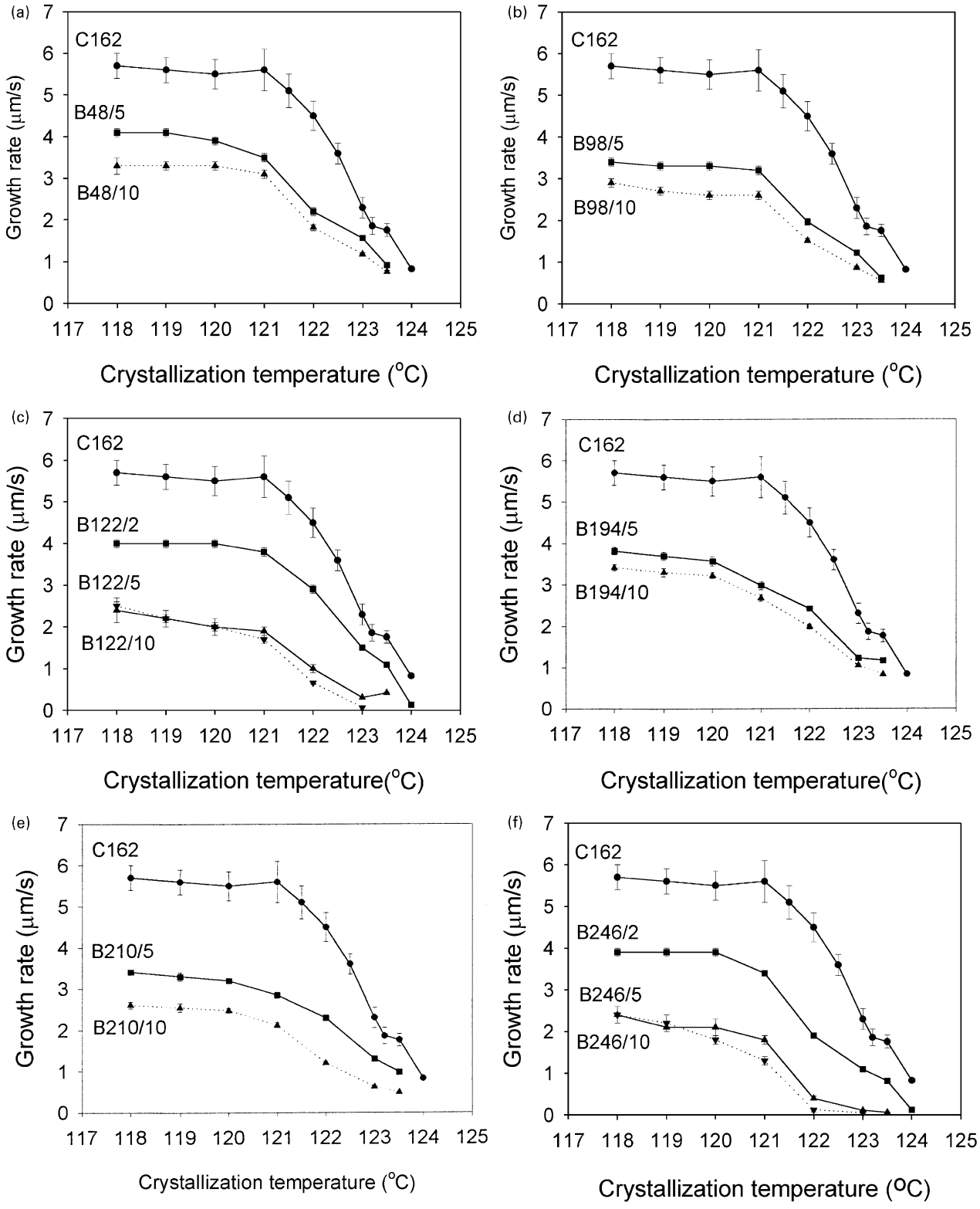

Fig. 2. Averaged growth rates as a function of crystallization temperature and composition for blend sets as labelled.

any figure (corresponding to differing amounts of the same guest molecule), the absolute value of growth rate always decreases with increasing proportion of guest. Moreover, when different guest molecules are compared at a fixed molar percentage (say, 5%) a longer guest molecule causes a proportionately larger decrease in growth rate: compare, for instance, B210/5 and B246/5. These general trends are also substantially reproduced above 120°C with some of the

blends following broadly the same behaviour, namely B194/5 and B246/2; B194/10 and B210/5; finally, B210/10, B246/5 and B246/10, falling to values which again appear to represent some minimum growth rate at a given temperature.

This is not the whole story, as blends B194/5 and B246/2, for example, have a similar temperature-dependent growth rate despite containing approximately 6 and 3 mass% of the guest alkane, respectively (Table 1). Moreover, blends B210/5 and B246/5 which both contain ~6 mass% of the guest alkane follow different curves. A detailed comparison of blends with the same nominal molar percentage of guest alkane, i.e. approximately the same number of guest alkane chains in each case, shows that for the same number of guest molecules, the longer one causes a correspondingly larger decrease in crystallization rates. Thus, both the amount and length of the guest molecule affect growth behaviour.

3.2. Melting behaviour

Melting endotherms of 10 mol% blends after isothermal crystallization at 118, 120 and 122°C are shown in Fig. 3 in order of increasing guest chain length. Those of the shorter guests, C48, C98 and C122, in Fig. 3a–c, respectively, all reveal these as separated low-melting populations, a feature never shown by blends with longer guest molecules because they co-crystallize. Note that for the shorter guest molecules, slight variations in peak shape are associated with the different sample masses used in each case. A larger sample mass tends to give a broader peak as in Fig. 3a (3 mg samples) in contrast to Fig. 3b and c (1 mg samples); the larger sample in the former case was necessary to resolve the smaller mass of the C48 guest. Only blends with C122 show some multiplicity in the melting of the segregated population. At 118°C (just below the melting point of C122 at 119°C), they always show a degree of co-crystallization. At higher crystallization temperatures, segregation occurs without complication (Fig. 3c) and is slightly more efficient at the highest temperatures as indicated by the increasing prominence of the minor peak. Note finally that the magnitude of the minor peak increases with the length of the minor component, as is to be expected for the increasing mass implied by constant molar percentage (Table 1).

When the relevant masses are taken into consideration, the specific enthalpy of the peak associated with the melting of the host alkane in blends with shorter guests is in line with that expected (200–220 J g^{-1}) of the pure host. Similarly, when a longer alkane is used with the host (Fig. 3d–f), the specific enthalpies of the single peaks are broadly in line with that expected (~210 J g^{-1}) and with those reported for similar blends [10,11]. These single endotherms are located at ~400 K, the temperature expected for pure C162. No deviations were detected within the resolution of the instrument nor was there ever any evidence of a second peak corresponding to a separate crystal population of the guest alkane in these systems, even when they were quenched directly from the melt. This is clear evidence of co-crystallization, carrying with it the implication of permanent ciliation of the C162 crystals by the longer guest molecules.

3.3. Morphology

3.3.1. Optical micrographs

Representative optical appearances, between crossed polars, of various blends with shorter guest molecules, all crystallized at 120°C, are displayed in Fig. 4. The host (Fig. 4a) shows a texture of *pseudo-spherulites*, that is objects containing packets of parallel lamellae radiating from common centres, with well-defined boundaries and so lacking the distinctive 'Maltese cross' associated with classic spherulites. Blend B48/5 (Fig. 4b), which contains only 1.5% by mass of the guest alkane, is distinctly less ordered but has some pseudo-spherulites still distinguishable. The object size is somewhat reduced indicative of enhanced primary nucleation. Blend B98/5 (Fig. 4c), containing 3 mass% of the guest alkane, shows smaller, more randomly oriented packets of lamellae in a texture now lacking any clear radial symmetry. Similar, but less divergent, arrays are present in Fig. 4d, of blend B98/10 (containing 6% by mass of C98) with some evidence of a second, finer phase located between these objects e.g. right of centre. Blend B122/5 (Fig. 4e) has less mature objects, which show now some evidence of cellulation, the crystals adopting a 'ragged' appearance in a darker surrounding matrix of quenched material rich in C122. The crystals of blend B122/10 (Fig. 4f) are still less well developed with a more fragmented appearance in a wider expanse of the quenched matrix, through which some darker subsurface objects can be viewed. Such morphologies reveal a progressive departure, in an increasingly non-spherulitic sense, from the texture of the pure host as the amount of the segregating species is increased.

The opposite tendency is revealed in Fig. 5 for blends crystallized at 122°C showing that the addition of a longer guest molecule changes the morphology progressively towards that of classic spherulites with equivalent radii and associated Maltese crosses. The morphology of the host (Fig. 5a) is similar to that after crystallization at 120°C (as shown in Fig. 4a) but with larger objects because of the lower primary nucleation density at lower supercooling. Blend B194/5 (Fig. 5b) has a very similar, but somewhat finer, lamellar texture whereas in blend B194/10 (Fig. 5c) Maltese crosses are more distinct. Blend B210/5 has a similar intermediate texture (Fig. 5d), anticipating the distinctly spherulitic appearance with prominent Maltese crosses of blends B210/10 (Fig. 5e) and B246/10 (Fig. 5f).

3.3.2. TEM investigations

The lamellar details underlying the above gross changes in texture are revealed in the representative electron

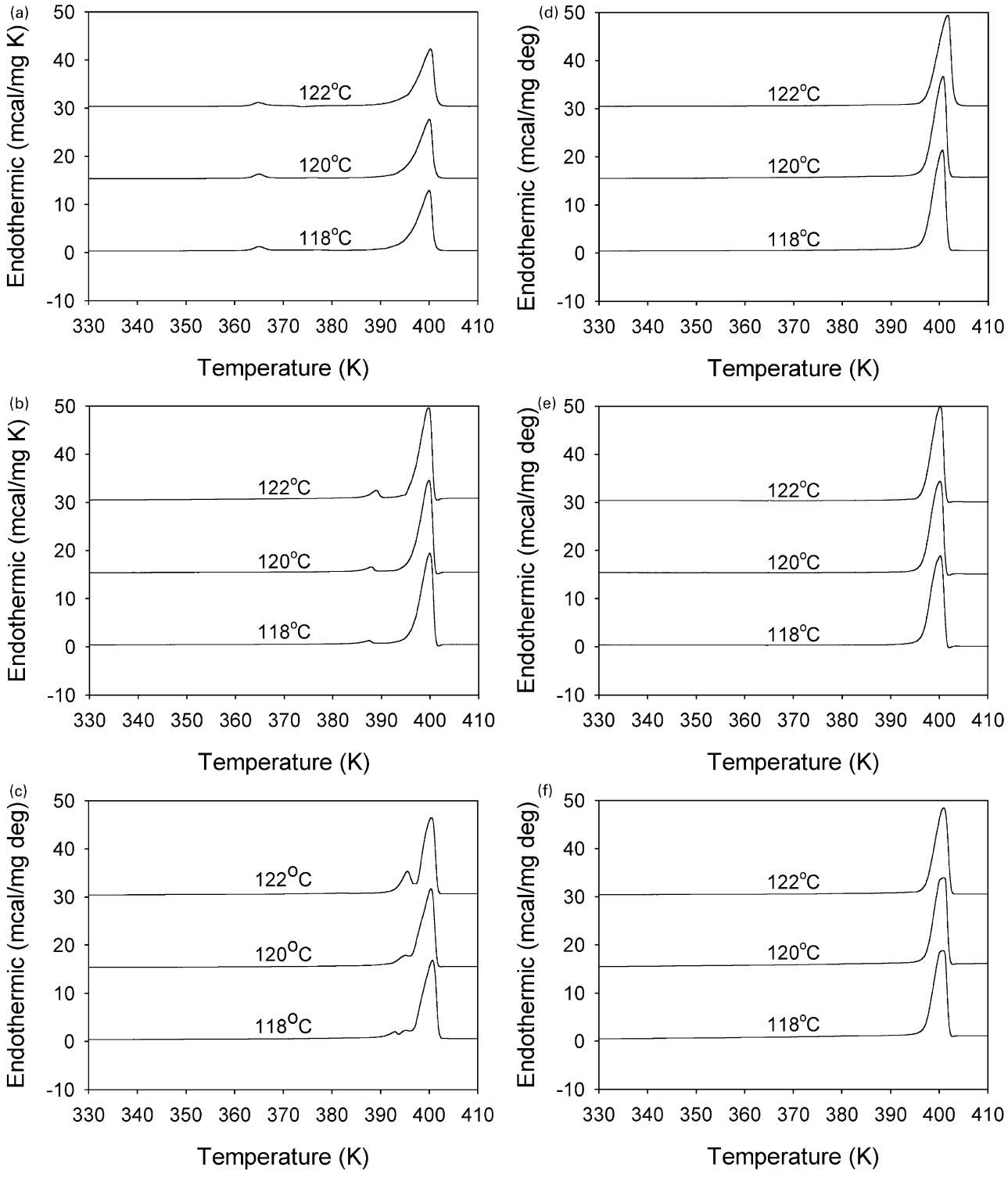

Fig. 3. DSC melting endotherms of blends taken after crystallization at the indicated temperatures for (a) B48/10, (b) B98/10, (c) B122/10, (d) B194/10, (e) B210/10 and (f) B246/10.

micrographs of Fig. 6. In the host alkane (Fig. 6a), the pseudo-spherulites show a degree of lamellar branching, usually confined to the earliest stages of development, so that the consequent crystals are usually very planar in nature following initial divergence. This texture is not too dissimilar to the blend B48/5 (Fig. 6b) which contains only 1.5 mass% of C48; here, the edge on objects are representative of the finite divergence angles experienced in this and all the alkane blends. In blend B122/10 (Fig. 6c), the morphology is one of broad

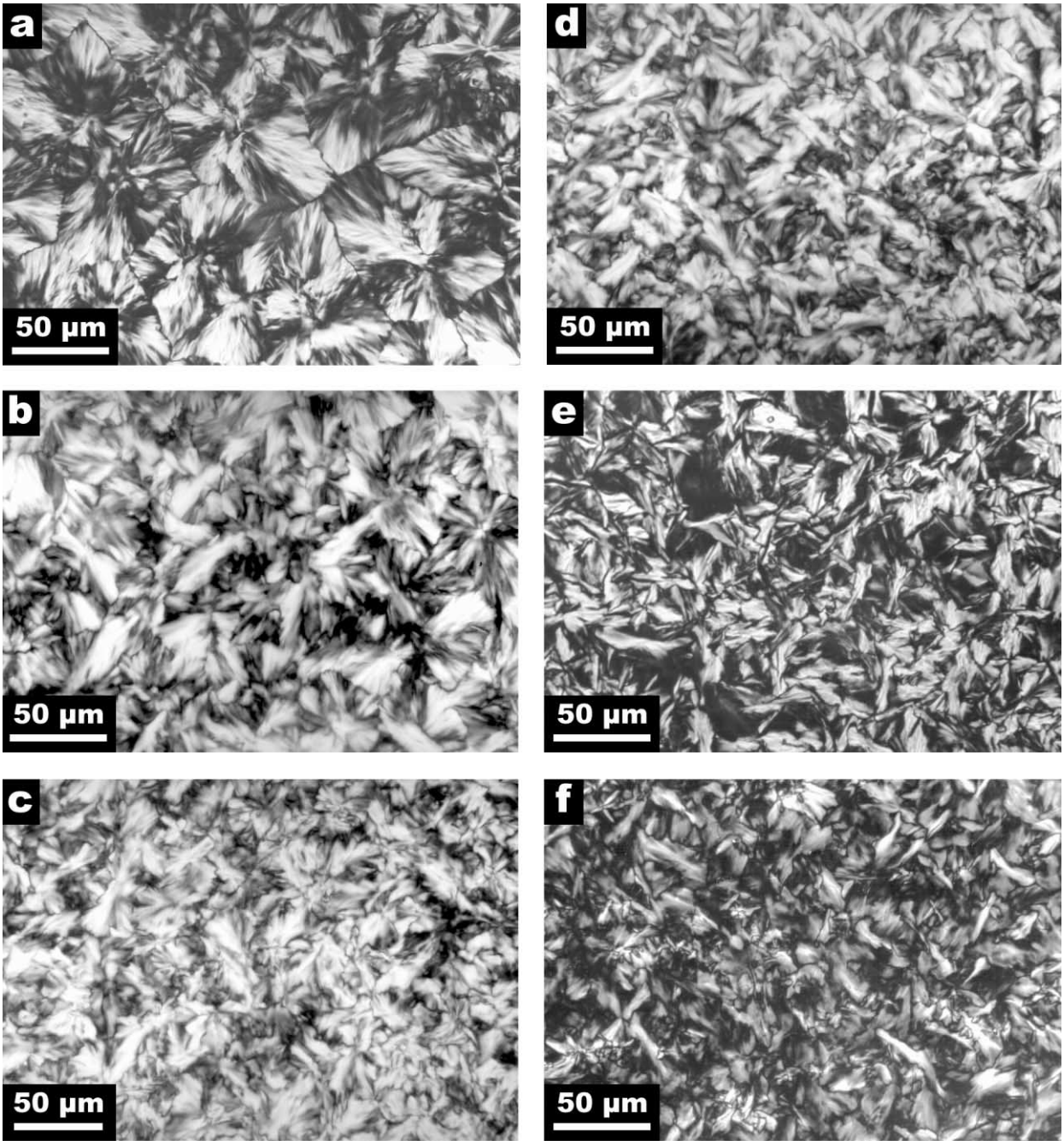

Fig. 4. Optical micrographs between crossed polars of C162 and blends with a shorter guest crystallized at 120°C: (a) pure C162, (b) B48/5, (c) B98/5, (d) B98/10, (e) B122/5, and (f) B122/10.

expanses of near-parallel lamellae showing less evidence of lamellar divergence.

The tendency towards spherulitic morphologies in blends with a longer guest molecule is exemplified in Fig. 6d of blend B194/5 containing objects whose lamellae continually diverge, making the gross habit curved contrary to that of the host (cf. Fig. 6a). Fig. 6e shows a typical object with spherulitic character in Blend B210/10 while Fig. 6f shows a divergent, sheaf-like object in blend B246/10; both show prominent radial, diverging lamellar textures.

3.4. Splaying angles

Fig. 7 shows the splaying angles between adjacent dominant lamellae plotted against the supercooling, calculated from 126.5°C, the melting point of C162(9). For the blends with shorter guest alkanes, the gradient decreases with the mass percentage of the guest alkane present (see Table 2) but the intercept remains constant at ~8°. With the longer guest alkanes, two things happen: first, the gradient is reduced in proportion to the mass of the guest alkane (and

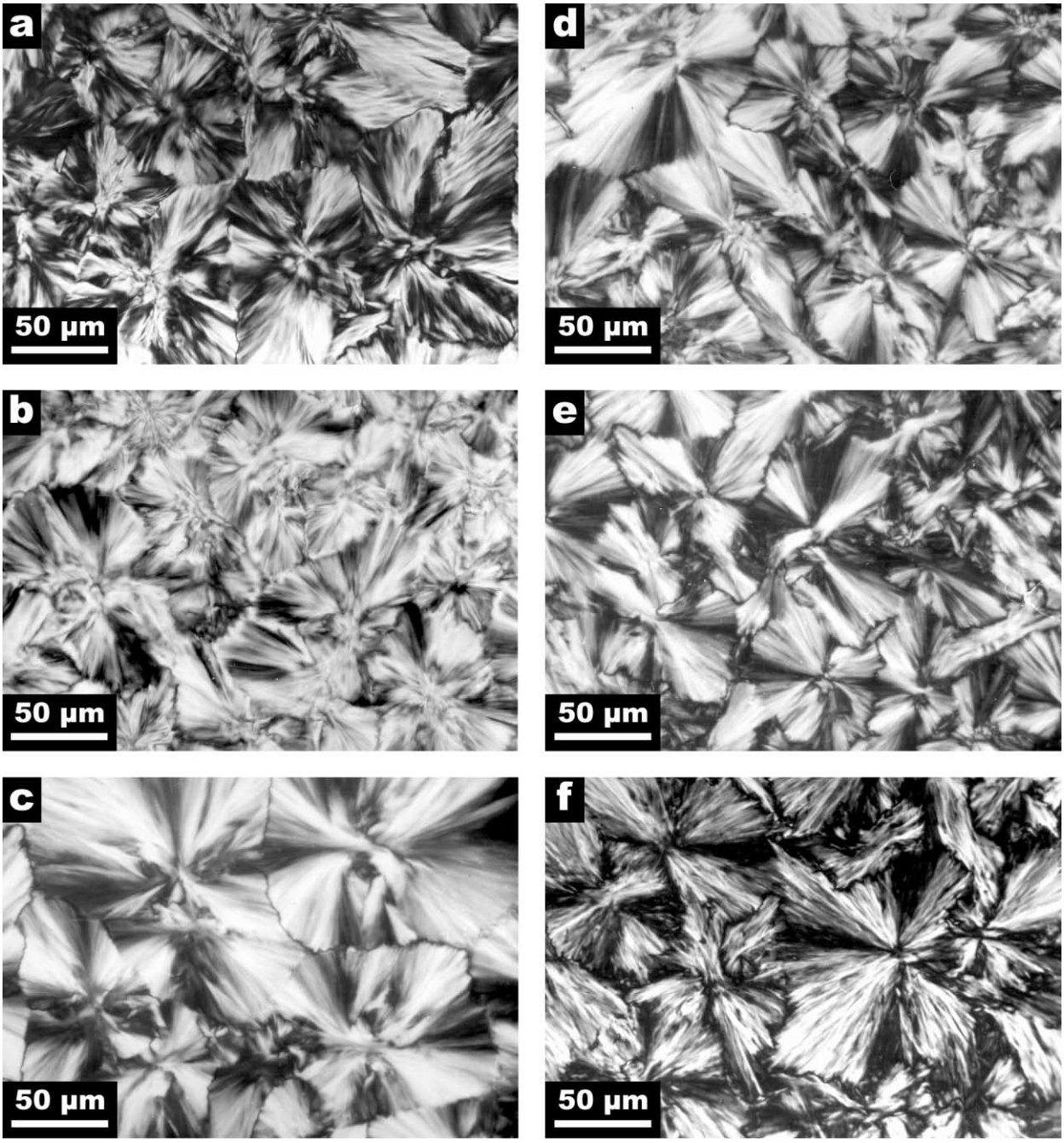

Fig. 5. Optical micrographs between crossed polars of C162 and its blends with longer guest alkanes crystallized at 122°C: (a) pure C162, (b) B194/5, (c) B194/10, (d) B210/5, (e) B210/10, and (f) B246/10.

shows a slight dependence on the length of that alkane, Table 2); second, the intercept is increased by an amount proportional to both the mass percentage and the length of the guest molecule. The significance of these features is discussed below.

4. Discussion

In the several papers in which we have examined the melt-crystallization of the monodisperse *n*-alkanes with a view to clarifying central features of comparable polymeric behaviour, it was first shown that spherulitic growth occurs for chainfolded, but not extended-chain growth of the same alkane, thereby confirming the involvement of transient cellulation [3,4]. This concept was then widened to account for the onset of lamellar divergence in extended-chain growth at higher supercoolings, which increases linearly with transient cilium length (defined as the excess of molecular length over that of the secondary nucleus), albeit with

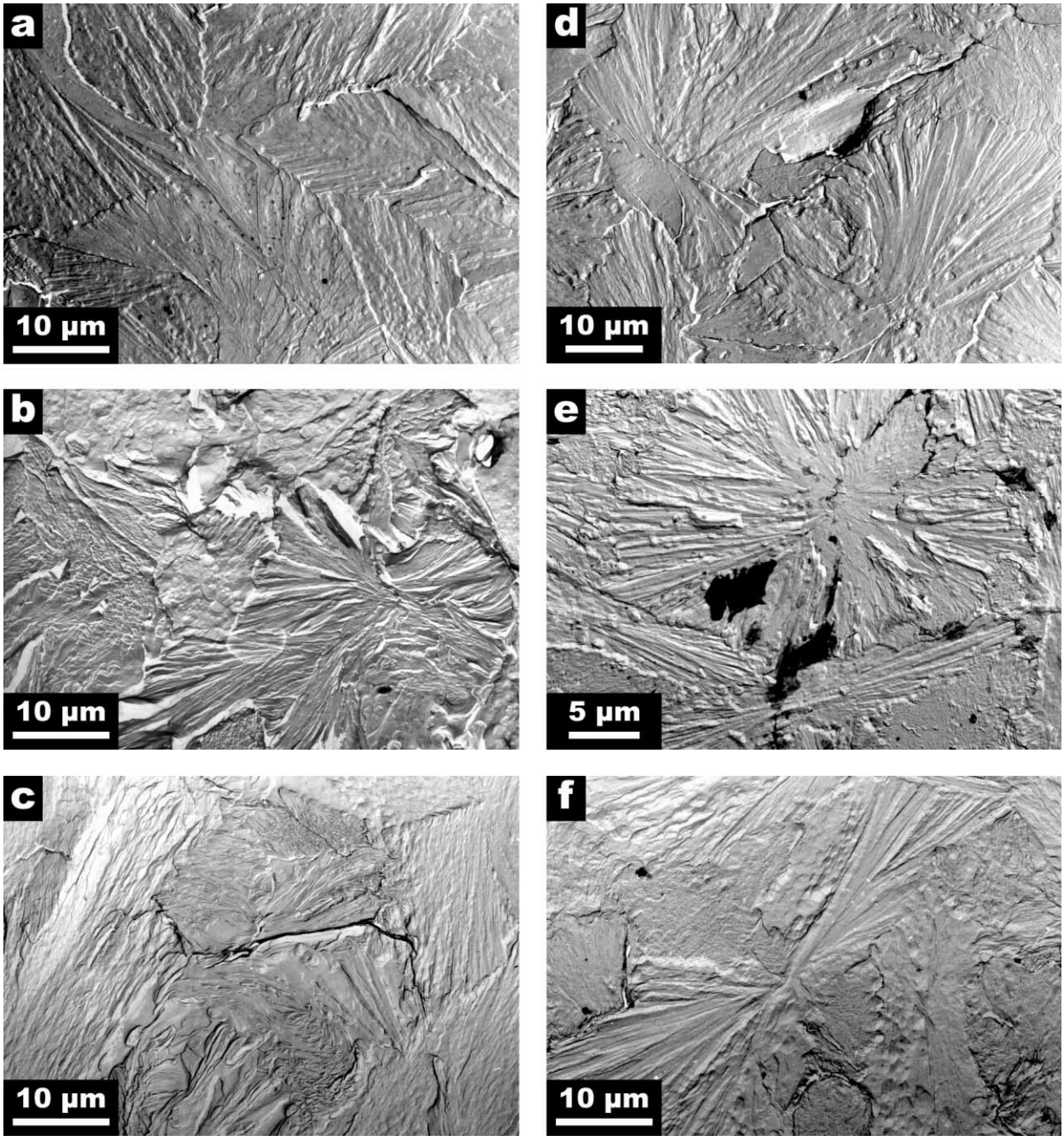

Fig. 6. TEM micrographs of pure C162 and selected blends crystallized at the stated temperatures: (a) C162 at 121°C, (b) B48/5 at 121°C, (c) B122/10 at 120°C, (d) B194/5 at 120°C, (e) B194/10 at 120°C and (f) B246/10 at 120°C.

finite divergence extrapolated to zero supercooling [8,9]. For this last feature, an additional mechanism is required: inclined packing of initially rough surfaces was proposed [10]. In all cases, transient ciliation was shown to promote both lamellar divergence and spherulitic growth, features which are disfavoured by segregation. Finally, the introduction of permanent ciliation was shown further to promote spherulitic growth with additional divergence at zero supercooling (a feature which disappears when the molecular length ratio precludes permanent cilia [11]).

This paper now examines the relative effects of a series of different guest molecules in dilute binary blends, i.e. of controlled permanent cilium length for longer guest molecules and variable segregation for shorter additives. The results illustrate especially the role of permanent ciliation with the additional lamellar splaying it causes being proportional to the number of cilia and increasing with cilium length. Moreover, details of the splaying/supercooling plots are shown to correspond consistently to different causes of lamellar divergence, namely transient

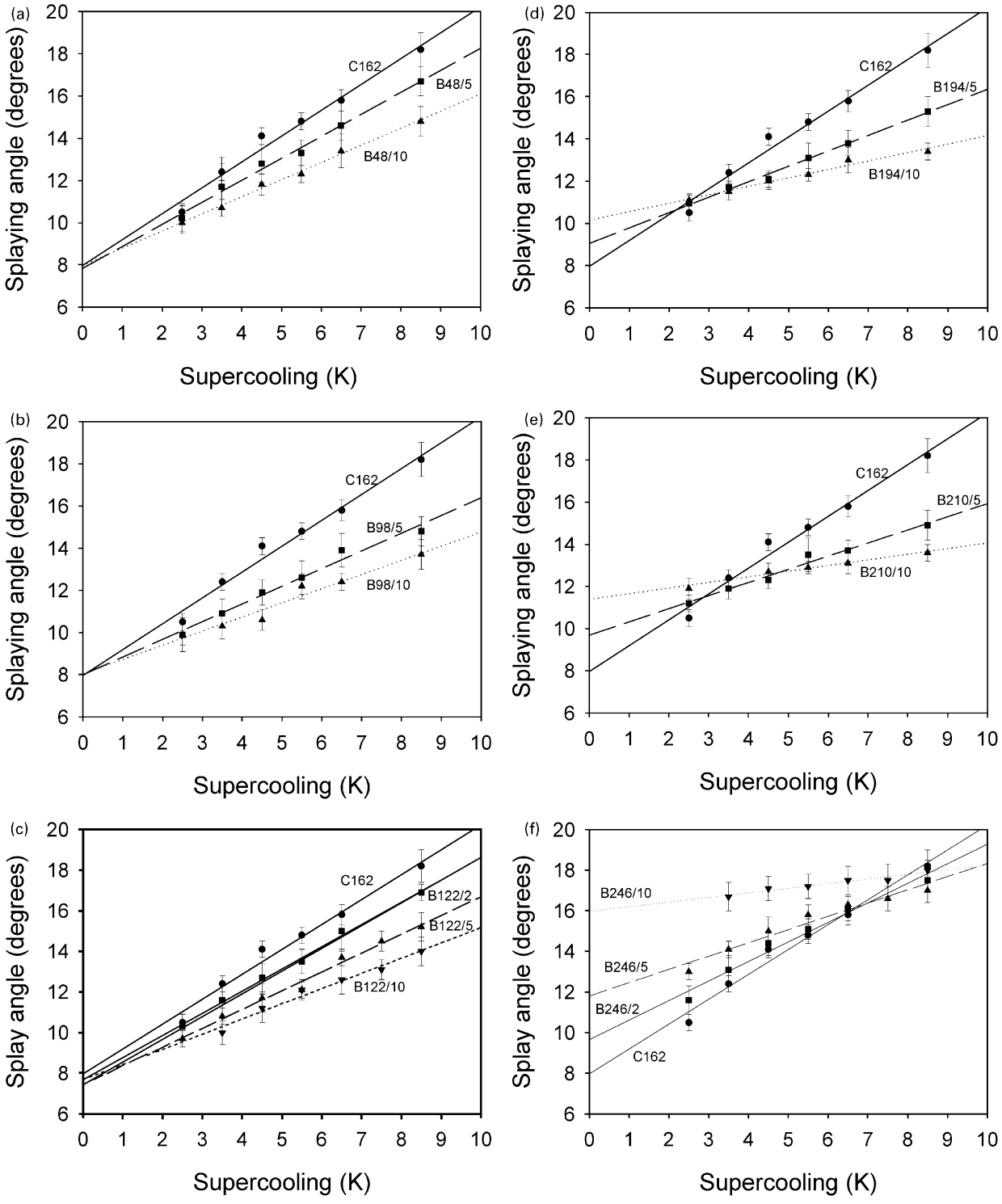

Fig. 7. Splaying angles as functions of supercooling for the pure host and specified blends.

ciliation, permanent ciliation and inclined packing of rough surfaces.

The principal features of crystallization are that under the conditions used, shorter guest molecules segregate giving non-linear kinetics, whereas longer ones co-crystallize with a constant, though reduced, rate compared to the host (Figs. 1 and 2). Optical textures of the former are less spherulitic, the latter more spherulitic than the host in the sense of movement towards the equivalent radii and concomitant Maltese crosses of classic spherulites (Figs. 4–6).

Table 2
Splaying angle data

Blend	Gradient, G (K^{-1}	G/G_0	$1 - G/G_0$	Intercept I (°)	$I - 8.0$
C162 host	1.23 ± 0.06; G_0	1.0	0.0	8.0 ± 0.2	
B48/5	1.04 ± 0.06	0.85	0.15	7.8 ± 0.2	
B48/10	0.81 ± 0.05	0.66	0.34	8.0 ± 0.2	
B98/5	0.84 ± 0.05	0.68	0.32	8.0 ± 0.2	
B98/10	0.67 ± 0.04	0.54	0.46	8.1 ± 0.2	
B122/2	1.09 ± 0.06	0.89	0.11	7.7 ± 0.2	
B122/5	0.92 ± 0.05	0.75	0.25	7.4 ± 0.2	
B122/10	0.75 ± 0.05	0.61	0.39	7.7 ± 0.2	
B194/5	0.73 ± 0.05	0.59	0.41	9.1 ± 0.2	1.1
B194/10	0.40 ± 0.05	0.33	0.67	10.2 ± 0.2	2.2
B210/5	0.62 ± 0.05	0.50	0.50	9.7 ± 0.2	1.7
B210/10	0.27 ± 0.04	0.22	0.78	11.4 ± 0.2	3.4
B246/2	0.96 ± 0.05	0.78	0.22	9.7 ± 0.2	1.7
B246/5	0.65 ± 0.04	0.53	0.35	11.8 ± 0.2	3.8
B246/10	0.23 ± 0.03	0.17	0.83	16.0 ± 0.2	8.0

Reductions in growth rate depend primarily on the total added mass of guest molecules rather than their length but, for longer additives, molecular (and thus permanent cilium) length is also a factor as described above.

The special novelty of this paper is the data of Fig. 7 and Table 2, which display four salient characteristics. First, there is the linearity of the plots against supercooling; second, the reduction in slope which scales approximately as the mass of the added molecules; third, there is the finite intercept at zero supercooling which is unaffected by segregation, and fourth there are the increases in intercept with both the number and length of longer guest molecules; we shall consider these in turn.

It has been pointed out previously [8] that the transient cilium length, taken to be the excess of molecular length over that of the secondary nucleus, is expected to increase linearly with supercooling. While given the small range of temperatures concerned, too much should not be read into this particular power law dependence, at face value, it suggests that more or less extended conformations of cilia are responsible for the repulsive pressure between adjacent lamellae which causes them to diverge but only in the near neighbourhood of their branch point. The progressive reduction in slope for increasing quantities of segregated guest molecules suggests that a dilution effect is coming into play with the number of effective transient cilia being reduced by the presence of the additive. A simple measure of the reductions of slope is the quantity $(1 - G/G_0)$, listed in Table 2, which compares each gradient, G, to that of the host, G_0. The reduction for the C48 blends is in line with the number of added molecules, otherwise, for C98 and C122, the decrease is less than proportionate and is smallest for C122, the least mobile segregant. Numerically greater reductions apply to the co-crystallizing blends with longer additives but these also fall off with the number of added molecules. The consistent linearity of the plots supports the concept that the number of effective transient cilia also has to be reduced when permanent cilia are present. It is notable that these reductions of slope, when either segregated shorter molecules or permanent cilia are located outside basal surfaces, stand in contrast to the maintained slope for C122/C246 blends for which folding of the longer guest at the same period as the host implies that there are no permanent cilia, and thus no interference with transient ciliation.

The finite extrapolated intercepts, I, in Fig. 7 are not explicable by transient ciliation, which will be zero at the melting point. Previously available data on different monodisperse *n*-alkanes have all given an intercept ~8°, consistent with the suggestion that it is a geometrical consequence of poor packing of initially rough surfaces, before surface ordering has attained the ideal planar condition. The striking data of Fig. 7a–c in which the intercept is unaffected by segregation suggest, therefore, that packing of such surfaces is not moderated by nearby segregated guest molecules.

Recent papers have shown that an increase in intercept, over the value for the host, appears when there are permanent cilia [10], produced by co-crystallization, but disappears again when a molecular length ratio of two precludes permanent ciliation [11] in co-crystallized lamellae. The responsibility of permanent cilia is clear, a conclusion reinforced by the data of Fig. 7d–f, showing that the additional intercept above that of the host, listed as $(I - 8)$ in Table 2, increases linearly with the number of permanent cilia, i.e. of guest molecules, in all three blends studied.

These figures also show an increase with the length of the permanent cilium. At fixed mol% of added guest, the values are higher for the longer molecules, more so than for the extra increments of length themselves, viz. 32, 48 and 84 C atoms. This indicates a power dependence on cilium length of between one and two, as would be expected when cilia move away from linear entities towards more random conformations. Protruding from basal surfaces as they must do, permanent cilia will cause lamellae to diverge more at their branch points over and above their existing misalignment ascribed to rough surfaces. The scenario outlined in which the gradient of splaying/supercooling plots relates to transient ciliation with the intercept informing on surface packing and permanent ciliation is both self-consistent and in agreement with the body and trends of rather comprehensive results.

The increased intercepts and decreased slopes of blends with longer guest molecules implies that, at higher supercoolings, splaying angles will fall below those of the host alkane, as Fig. 7 illustrates. The textural consequences will depend also on the frequency of branching: it is the product of this with splaying angle, which determines the rate of progression towards a spherical envelope. It may well be pertinent that, so far as the observed textures are concerned, the most pronounced move towards a spherulitic texture is for the blends with C246 for which, in the range studied, splaying angles are greater than for the host.

5. Conclusions

The principal conclusions of this work are as follows:

1. Blend behaviour differs according as the guest molecule is longer or shorter than the host, C162.
2. Shorter guest molecules segregate as a separate population, depressing the growth rate and making it non-linear. Corresponding textures are less spherulitic than the pure host with less lamellar divergence and no additional splaying.
3. Longer guest molecules co-crystallize with the C162 host creating permanent cilia while the radial growth rate remains linear, though depressed.
4. Permanent cilia give more spherulitic textures with additional splaying proportional to the number of cilia and increasing with their length.
5. Splaying vs. supercooling plots are linear with their gradients informing on the extent of transient ciliation. Permanent cilia are measured by the magnitude of the intercepts above that for the pure hosts (and segregated blends), which relates to the inclined packing of initially rough surfaces.

Acknowledgements

This research was funded by EPSRC under whose auspices the *n*-alkanes were synthesized and supplied by Dr G.M. Brooke and colleagues at the University of Durham.

References

[1] Paynter OI, Simmonds DJ, Whiting MC. J Chem Soc Chem Commun 1982:1165–6.
[2] Bidd I, Holdup DW, Whiting MC. J Chem Soc Perkin Trans 1 1987:2455–63.
[3] Bassett DC. CRC Crit Rev Solid State Mater Sci 1984;12:97–163.
[4] Bassett DC, Olley RH. Polymer 1984;25:935–43.
[5] Bassett DC, Vaughan AS. Polymer 1985;26:717–25.
[6] Bassett DC, Olley RH, Sutton SJ, Vaughan AS. Macromolecules 1996;29:1852–3.
[7] Bassett DC, Olley RH, Sutton SJ, Vaughan AS. Polymer 1996;37:4993–7.
[8] Teckoe J, Bassett DC. Polymer 2000;41:1953–7.
[9] Hosier IL, Bassett DC. Polymer 2000;41:8801–12.
[10] Hosier IL, Bassett DC, Vaughan AS. Macromolecules 2000;33:8781–90.
[11] Hosier IL, Bassett DC. J Polym Sci, submitted for publication.
[12] Abo el Maaty MI, Bassett DC. Polymer 2001;42:4965–71.